AIP | Applied Physics Letters

Temperature control in thermal microactuators with applications to in-situ nanomechanical testing

Qingquan Qin and Yong Zhu

Citation: Appl. Phys. Lett. **102**, 013101 (2013); doi: 10.1063/1.4773359
View online: http://dx.doi.org/10.1063/1.4773359
View Table of Contents: http://apl.aip.org/resource/1/APPLAB/v102/i1
Published by the American Institute of Physics.

Temperature control in thermal microactuators with applications to *in-situ* nanomechanical testing

Qingquan Qin and Yong Zhu[a)]
Department of Mechanical and Aerospace Engineering, North Carolina State University, Raleigh, North Carolina 27695, USA

(Received 1 October 2012; accepted 6 December 2012; published online 2 January 2013)

Thermal microactuators are used in many micro/nano-technologies. To circumvent undesired heating of the end effector, heat sink beams are co-fabricated with the thermal actuator and connected to the substrate. This paper reports a combined experimental and modeling study on the effect of such heat sink beams. Temperature distribution is measured and simulated using Raman scattering and multiphysics finite element method, respectively. Our results show that heat sink beams are effective in controlling the temperature of the thermal actuator. Insights on how to achieve both low temperature and large actuator displacement for *in-situ* mechanical testing of nanoscale specimens are provided. © *2013 American Institute of Physics*.
[http://dx.doi.org/10.1063/1.4773359]

In the field of microelectromechanical systems (MEMS), electrothermal actuators (ETAs) have emerged as structurally simple, compact, stable, and high-force actuation apparatuses.[1–4] ETAs have been exploited in a variety of configurations to achieve desired in-plane motion, such as U-shape,[1] V-shape,[2,3] and Z-shape.[4] They are used in a broad range of applications, including on-chip nanoscale material testing systems,[5,6] micromotors,[7] microtweezers,[8] and bistable mechanisms.[9] The ETAs are heated to high temperature (e.g., hundreds of degree Celsius), which might limit their applications and thus invokes the need to control the actuator temperature, especially at the end where end effector is attached. Due to constraints in microfabrication, solutions to dissipate the heat are limited. One solution was to leave cuts in the ETAs and fill with dielectric spacers,[3] which however inevitably caused additional fabrication steps.

Of particular interest is the mechanical testing of nanostructures using ETAs. MEMS offer unprecedented opportunities for quantitative *in-situ* electron microscopy testing of nanostructures.[10] ETAs provide stable, displacement-controlled loading, and become widely used for nanomechanical testing. However, the mechanical behavior can be affected by temperature (e.g., for silicon[11]). To circumvent the heating problem, Zhu *et al*.[6] introduced so-called heat sink beams as a simple solution. Though predicted by modeling, the effect of such a design has not been verified by any experiments. In fact, the modeling treated only the vacuum condition, while temperature measurement of MEMS devices is typically conducted in air. Generally speaking, although a large amount of modeling work has been devoted to ETAs, heat dissipation to air is either neglected[12] or considered in specific cases (e.g., heat conduction through air to substrate),[13] with very few exceptions.[14]

In this paper, we report experimental measurement and multiphysics modeling of the temperature profile of a V-shaped ETA; Figure 1 shows a scanning electron microscopy (SEM) image of the ETA. The temperature measurement was based on Raman scattering in air. Fully 3D multiphysics (coupled electrical-thermal-mechanical) simulation was used to treat both the air and vacuum conditions; the air and vacuum conditions are of relevance to the Raman measurement and the *in-situ* electron microscopy testing of nanostructures, respectively. For the same ETA, the Raman measurement and multiphysics modeling were carried out with and without the heat sink beams; the heat sink beams were carved out by focused ion beam (FIB). Our results demonstrated that the heat sink beams play a critical role in reducing the temperature in the ETA.

The ETAs were fabricated at MEMSCAP (Durham, NC) using the Silicon-on-Insulator Multi-User MEMS Processes (SOI-MUMPs).[4] Dimensions of an ETA are summarized in Table I. The temperature measurements were conducted using a HORIBA LabRAM HR Raman microscope in air (laser wavelength 633 nm). The laser power was kept below 0.003 mW to avoid laser-induced local heating. The Raman

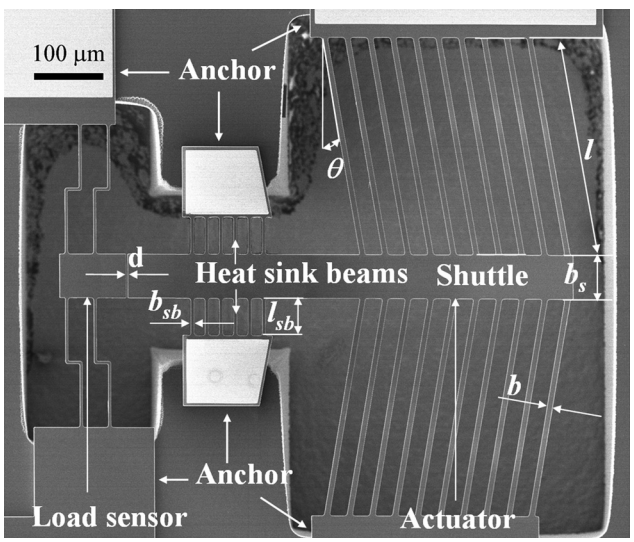

FIG. 1. SEM image of a nanomechanical testing stage including a V-shaped ETA (on the right), a load sensor (on the left), and a gap in between where nanostructures are mounted.

[a)]E-mail: yong_zhu@ncsu.edu.

TABLE I. Dimension of the SOI V-shaped ETA.

Dimension	Symbol	Value	Unit
Inclined beam length	l	296	μm
Inclined beam width	b	8	μm
Gap between actuator and sensor	d	2	μm
Inclination angle	θ	10	deg.
Heat sink beam length	l_{sb}	50	μm
Heat sink beam width	b_{sb}	5	μm
Shuttle length	l_s	627	μm
Shuttle width	b_s	60	μm
Thickness	t	10	μm
Gap between device and substrate	g	400	μm

signal was collected in backscatter through the microscope objective, relayed to a grating spectrograph, and detected using a deep-depletion, thermoelectrically cooled CCD camera. Each measurement took approximately 60 s.

Figure 2 shows the Stokes-shifted Raman spectra of a representative position (620 μm from the specimen edge) on the ETA at four different temperatures. Several features were observed with increasing temperature: (1) the position of the Raman peaks is shifted toward lower phonon energies, (2) the Raman lines broaden, and (3) the intensity of the anti-Stokes signature relative to the Stokes-shifted line increases. Kearney *et al.*[15] found the peak position of the Stokes-shifted Raman spectrum to be a robust indicator of temperature compared to the other two signals, therefore, the Stokes shift was recorded and analyzed in our experiments. The Raman spectra were fit to a Voight lineshape function to determine the Stokes peak location. It is seen that with increasing actuation voltage, the Stokes peak blue-shifted.

To quantify the effect of the heat sink beams, the Raman spectra were obtained on the same ETA with and without heat sink beams (see Figures 1 and S1 for contrast). Following the calibration experiment (see supplemental material for details[20]), the change in the peak position can be converted to the temperature rise in the ETA, viz.,

$$\Delta T = \frac{\Omega - \Omega_0}{-0.0242\,\mathrm{cm}^{-1}} \frac{K}{}, \tag{1}$$

where Ω_0 and Ω are the measured peak positions at the laboratory temperature of 296 K and at the operating temperature, respectively.

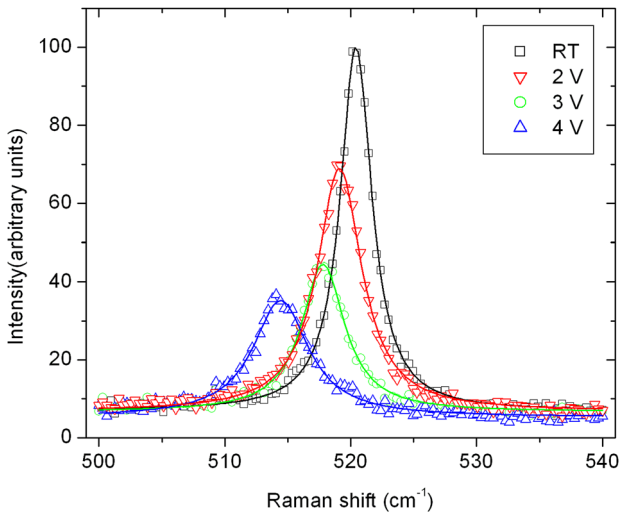

FIG. 2. Raman spectra of an ETA at room temperature and three different actuation voltages. Note that the spectra shown are fitted to a Voight lineshape function.

Nonlinear multiphysics finite element analysis (FEA) was carried out using ANSYS 13.0 to study temperature distribution of the ETA both in vacuum and in air. For the vacuum condition, the only heat dissipation mechanism is the heat conduction through the device itself to the anchors (substrate). For the air condition, additional heat dissipation mechanism is thermal conduction through the air to the substrate and neighboring devices. We found that thermal convection and thermal radiation are negligible.

The simulation is a coupled-field analysis involving electric, thermal, and mechanical fields. The thermal boundary conditions are zero temperature change at the anchors for the vacuum condition, but additionally at the surrounding substrate and the neighboring device (e.g., the load sensor to the left of the actuator in Figure 1) for the air condition. The mechanical boundary conditions are fixed displacements at the anchor sites. Element type SOLID 98 was used for the ETA and SOLID 70 was used for the air. The laboratory temperature during the RAMAN experiments (296 K) is set as the reference temperature in the simulations. The material parameters used in the simulations are listed in Table II.

Figures 3(a) and 3(b) show the temperature distributions of an ETA without and with heat sink beams in vacuum, respectively. Without the heat sink beams, the only heat

TABLE II. Material parameters used in the simulations.

Parameter	Symbol	Value	Unit
Young's modulus[a]	E	160	GPa
Poisson ratio[a]	v	0.28	…
Thermal conductivity of Si[b]	$K_{Si}(T)$	$210658 \times T^{-1.2747}$	W/(m K)
Thermal conductivity of air[c]	K_{air}	0.026	W/(m K)
Free convection coefficient of air[d]	C_{air}	20	W/(m^2 K)
Thermal expansion coefficient[e]	$\alpha(T)$	$-4 \times 10^{-12}T^2 + 8 \times 10^{-9}T + 4 \times 10^{-7}$	K^{-1}
Resistivity[a]	$\rho(T)$	$5.1 \times 10^{-5}[1 + 3 \times 10^{-3}(T - 273)]$	Ωm

[a]Reference 4.
[b]Reference 16.
[c]Reference 17.
[d]Reference 18.
[e]Reference 19.

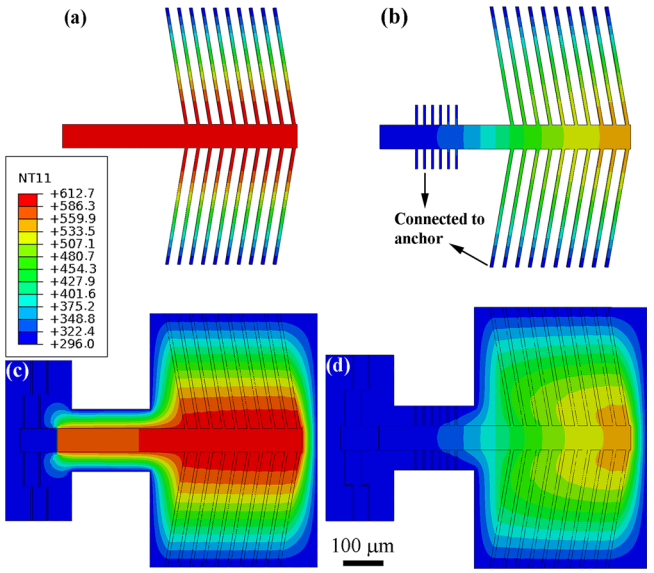

FIG. 3. Temperature distributions of an ETA under 4 V actuation voltage. (a) Without heat sink beam in vacuum, (b) with 6 pairs of heat sink beams in vacuum, (c) without heat sink beam in air, and (d) with 6 pairs of heat sink beams in air. For all the simulations, the thermal beams and heat sink beams are connected to the anchors, which are indicated in Figure 1. The temperature at the specimen end is (a) 612.7 K, (b) 315.6 K, (c) 572.5 K, and (d) 315.2 K, respectively.

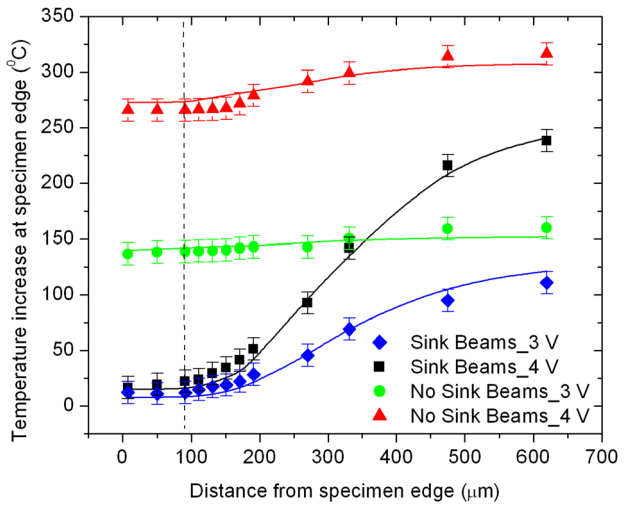

FIG. 4. Raman measurement and FEA of the temperature profile along the shuttle (starting from the specimen edge) under two different actuation voltages. Solid lines represent the FEA results and dots represent Raman measurements. The dashed vertical line shows the position of the nearest pair of heat sink beams (from the specimen edge).

dissipation path is to the two anchors of the ETA through the inclined beams. As a result, the highest temperature is in the shuttle. With the addition of the heat sink beams to the specimen end, more heat dissipation paths are provided (i.e., through the heat sink beams to the anchors). Hence the temperature of the shuttle at the specimen end is significantly reduced. In addition, the highest temperature in the ETA is lower than that without the heat sink beams.

Figures 3(c) and 3(d) show the temperature distributions of the ETA without and with heat sink beams in air, respectively. Without the heat sink beams, the temperature distribution is similar to that in vacuum, except that the temperature at the specimen end is considerably lower. The temperature continuously decreases along the shuttle from the opposite end (605 K) to the specimen end (573 K). This is mainly due to the heat conduction to the load sensor on the left side through the air gap. This heat dissipation is quite significant (i.e., causing ~40 K difference at the specimen edge) and cannot be captured in the previous thermal models.[13] With the heat sink beams, the temperature distribution is nearly identical to that in vacuum. Since the temperature at the specimen end is already very low even in vacuum, the heat conduction through the air gap is insignificant.

Figure 4 shows the measured temperature profiles along the shuttle (starting from the edge of the sample end) under two different actuation voltages, which agree very well with the simulation results for the air condition. With the heat sink beams, the temperature changes markedly along the shuttle length. In contrast, without the heat sink beams, the temperature only changes little along the shuttle length. This confirms the critical role that the heat sink beams play in reducing the temperature at the specimen end. There is a notable discrepancy in temperature (~15 K) between the experiments and simulations, especially at high temperature. The discrepancy might come from both experiments and simulations. Experimentally, alignment drift of the optical system, the accuracy in determining position of Raman peak, and the slope of calibration curve fit might cause errors.[15] Numerically, material parameters especially temperature dependent parameters might not be accurate.

For many applications such as the nanomechanical testing, ETAs often need to have both a low temperature increase and reasonably large travel range at the specimen edge. To gain insights for proper design of ETAs, additional FEA were employed to assess the effects of several parameters (number of thermal beams m, number of heat sink beams n, inclination angle θ, and length of heat sink beams l_{sb}). The simulations were performed in vacuum as it is relevant for *in-situ* electron microscopy nanomechanical testing. Note that no specimen was attached to the ETA in these simulations. Analytical approximation showing the ETA displacement as a function of these parameters was provided elsewhere.[6] Several guidelines can be drawn as follows (cf. Figure 5): (1) The larger m, the larger the displacement at a given temperature rise at the specimen edge. In this case, the temperature in the ETA remains nearly constant for a given applied voltage, while the driving force due to thermal expansion and thus the displacement both increase. (2) The larger n, the larger the displacement at a given temperature rise at the specimen edge. This seems in contrary to the first point. Though more heat sink beams increase the overall stiffness, they lead to drastically reduced temperature at the specimen edge. (3) As long as the length of the inclined beams does not change, the temperature in the ETA is independent of θ. Without the heat sink beams, the ETA displacement increases with the decreasing θ until ~5°, conservatively speaking (when $\theta < 5°$, the ETA might buckle), because the reduction in stiffness outweighs the reduction in driving force.[6] But with the addition of the heat sink beams, the reduction in stiffness is not that gainful any more. As shown in Figure 5, inclination angles of 5° and 10° yielded about the same results. (4) It is advisable to have relatively short heat sink beams. Though smaller l_{sb} leads to larger

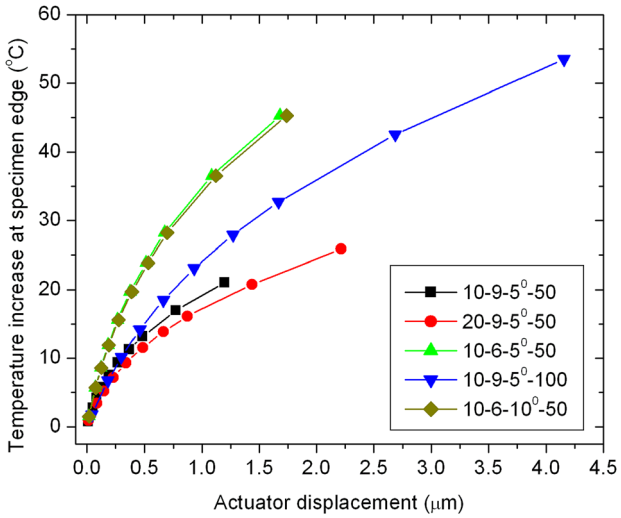

FIG. 5. Temperature increase versus displacement at the specimen edge under four different parameters (number of thermal beams m, number of heat sink beams n, inclination angle θ, and length of heat sink beams l_{sb}). In the legend, the four values are in the order of m, n, θ, and l_{sb}. All simulations were performed in vacuum with actuation voltage up to 7 V.

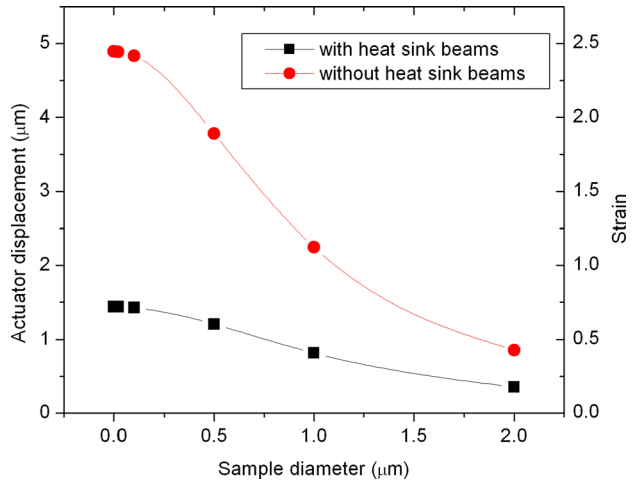

FIG. 6. Displacement results of the ETA (20-9-5°-50) actuated at 6 V for Si specimens ($E_{NW} = 160$ GPa, $L_{NW} = 2\,\mu$m) with different diameters. The heat sink beams are 9 pairs and 50 μm long.

stiffness of the overall device, they dissipate more heat and thus reduce the temperature at the specimen edge. Overall, 20 pairs of thermal beams, 9 pairs of heat sink beams, 5° or 10° inclination angle, and 50 μm heat sink beams were found to offer the best performance (cf. Figure 5).

The tradeoff of adding the heat sink beams is, however, the decreasing efficiency in loading (or actuating) the specimen. A considerable fraction of the heat (power) is dissipated through the heat sinks, which lowers the ETA temperature for a given voltage. In addition, part of the load applied by the ETA is distributed to the heat sink beams. To address this concern, we performed FEA with specimens of different diameters attached to the ETA under two cases: with (9 pairs 50 μm long) and without heat sink beams. As an example, we used a silicon specimen (2 μm long, circular cross section and $E = 160$ GPa). For an ETA with twenty 5° inclined thermal beams, Figure 6 shows the ETA displacement (at the specimen edge) as a function of the specimen diameter. The addition of heat sink beams dramatically decreases the ETA displacement. But the temperature increase at specimen edge also dramatically decreases from 823 to 21 °C (not shown). Even for the largest diameter of 2 μm, the ETA still moves 0.35 μm with the presence of the heat sink beams, corresponding to a strain of 17.5% on the specimen. Therefore, the reduced loading efficiency is not an issue for nanoscale specimens (e.g., nanowires with diameters less than 100–200 nm) or microscale specimens with relatively short length. For long microscale specimens (e.g., $\gg 2\,\mu$m), such reduced loading efficiency should be taken into account. FEA could be carried out to optimize the device performance (in terms of loading efficiency and temperature control).

In summary, we report experimental measurement and multiphysics modeling of the temperature profiles of a V-shaped ETA in the cases of with and without the heat sink beams. The Raman measurement of temperature agreed very well with the modeling results in air. Heat conduction through air to neighboring devices is considerable, while heat convection to the air is negligible. Our work unambiguously demonstrated that the heat sink beams play a critical role in reducing the temperature at the specimen end of the ETA. To reach reasonably large actuator displacement while maintaining low temperature, several design guidelines are provided including more inclined thermal beams, more heat sink beams, small inclination angle, and relatively short heat sink beams. These guidelines will be valuable to design ETAs for *in-situ* nanomechanical testing. It should be cautioned that while mitigating the undesired heating problem, heat sink beams also reduce the loading efficiency of the ETAs. The combined experiment-modeling methodology presented here can be applied to other MEMS devices where temperature control is desired.

This project was supported by the National Science Foundation under Award No. CMMI-1030637. The SEM and FIB experiments were performed in the Analytical Instrumentation Facility at North Carolina State University.

[1]J. H. Comtois and V. M. Bright, paper presented at the Solid State Sensors and Actuators Workshop, Hilton Head, SC, USA, 1996.
[2]R. Cragun and L. L. Howell, paper presented at the ASME International Mechnical Engineering Congress and Exposition, MEMS, 1999.
[3]L. Que, J. S. Park, and Y. B. Gianchandani, J. Microelectromech. Syst. **10**(2), 247 (2001).
[4]C. H. Guan and Y. Zhu, J. Micromech. Microeng. **20**, 085014 (2010); J. Ouyang and Y. Zhu, J. Microelectromech. Syst. **21**, 596 (2012).
[5]Y. Zhu, N. Moldovan, and H. D. Espinosa, Appl. Phys. Lett. **86**, 013506 (2005); Y. Zhu and H. D. Espinosa, Proc. Natl. Acad. Sci. U.S.A. **102**(41), 14503 (2005); S. S. Hazra, M. S. Baker, J. L. Beuth, and M. P. de Boer, J. Micromech. Microeng. **19**(8), 082001 (2009); M. S. Steighner, L. P. Snedeker, B. L. Boyce, K. Gall, D. C. Miller, and C. L. Muhlstein, J. Appl. Phys. **109**(3), 033503 (2011); A. Corigliano, L. Domenella, and G. Langfelder, Exp. Mech. **50**(6), 695 (2010).
[6]Y. Zhu, A. Corigliano, and H. D. Espinosa, J. Micromech. Microeng. **16**(2), 242 (2006).
[7]J. S. Park, L. L. Chu, A. D. Oliver, and Y. B. Gianchandani, J. Microelectromech. Syst. **10**(2), 255 (2001); J. M. Maloney, D. S. Schreiber, and D. L. DeVoe, J. Micromech. Microeng. **14**(2), 226 (2004).
[8]J. K. Luo, A. J. Flewitt, S. M. Spearing, N. A. Fleck, and W. I. Milne, J. Micromech. Microeng. **15**(6), 1294 (2005).
[9]M. S. Baker and L. L. Howell, J. Microelectromech. Syst. **11**(5), 566 (2002).
[10]M. A. Haque and M. T. A. Saif, Exp. Mech. **42**(1), 123 (2002); Y. Zhu, C. Ke, and H. D. Espinosa, Exp. Mech. **47**(1), 7 (2007).
[11]W. Kang and M. T. A. Saif, "In Situ Study of Size and Temperature Dependent Brittle-to-Ductile Transition in Single Crystal Silicon,"

Adv. Funct. Mater. DOI: 10.1002/adfm.201201992 (published online); Y. Zhu, F. Xu, Q. Qin, W. Y. Fung, and W. Lu, Nano Lett. **9**, 3934 (2009); F. Östlund, K. Rzepiejewska-Malyska, K. Leifer, L. M. Hale, Y. Tang, R. Ballarini, W. W. Gerberich, and J. Michler, Adv. Funct. Mater. **19**(15), 2439 (2009).
[12]Q. A. Huang and N. K. S. Lees, J. Micromech. Microeng. **9**(1), 64 (1999).
[13]C. D. Lott, T. W. McLain, J. N. Harb, and L. L. Howell, Sens. Actuators, A **101**(1–2), 239 (2002).
[14]A. Corigliano, L. Domenella, H. D. Espinosa, and Y. Zhu, Sens. Lett. **5**(3–4), 592 (2007); B. Pant, S. Choi, E. K. Baumert, B. L. Allen, S. Graham, K. Gall, and O. N. Pierron, Exp. Mech. **52**(6), 607 (2012).
[15]S. P. Kearney, L. M. Phinney, and M. S. Baker, J. Microelectromech. Syst. **15**(2), 314 (2006).
[16]L. Li and D. Uttamchandani, J. Micromech. Microeng. **19**, 075014 (2009).
[17]E. W. Lemmon, *CRC Handbook of Chemistry and Physics*, 92nd ed. (CRC Press, 2011), pp. 6–17.
[18]J. Vlachopoulos and D. Strutt, *Plastics Technician's Toolbox* (Society of Plastics Engineers, 2002), Vol. 2, pp. 21–33.
[19]A. A. Geisberger, N. Sarkar, M. Ellis, and G. Skidmore, J. Microelectromech. Syst. **12**, 513 (2003).
[20]See supplementary material at http://dx.doi.org/10.1063/1.4773359 for temperature calibration experiments.